JOURNAL OF MATERIALS SCIENCE **35** (2000) 1957–1971

Probing the early-stage/rapid processes in hydrolysis and condensation of metal alkoxides

M. Z.-C. HU*, J. T. ZIELKE, C. H. BYERS
Chemical Technology Division, Oak Ridge National Laboratory,‡ Oak Ridge, Tennessee 37831-6224, USA

J. S. LIN
Solid State Division, Oak Ridge National Laboratory, Oak Ridge, Tennessee 37831, USA

M. T. HARRIS
Department of Chemical Engineering, University of Maryland at College Park, College Park, Maryland 20742, USA
E-mail: i5h@ornl.gov

Understanding and control of the early-stage sol-gel reaction processes involving metal alkoxides are important to many advanced materials development and applications. In this work, Fourier transform infrared spectroscopy (FTIR) and small angle X-ray scattering (SAXS) were coupled with a specially designed, rapid flow-through mixing cell for monitoring such processes. The rapid, early-stage hydrolysis and condensation of zirconium *n*-butoxide in ethanol were chosen as the basis for a model system. FTIR was used to study soluble-species reaction kinetics, while the SAXS technique monitored in situ the solid-phase particle formation/growth (i.e., the nucleation and aggregation kinetics of polymeric clusters/particles). Monitoring the reactions and cluster/particle growth within a millisecond time regime was achieved. In addition, key parameters such as reaction time, concentration of base (i.e., quarternary tetramethyl ammonium hydroxide), temperature, water concentration, and alkoxide concentration were fully investigated in a continuous flow-through reactor.

1. Introduction

Sol-gel processing with the use of alkoxides as precursors has gained a significant level of interest in the past years for the production of advanced materials. One of the main advantages of the sol-gel process is that it allows careful control of the size and morphology of clusters/particles in the sol or gel during the early-stage processes, so that high-quality end products (in the form of powders, films, or coatings) can be developed to fulfill specific demands [1]. Some of the current applications of sol-gel process involve the development of a new generation of advanced materials for structural, electrical, optical, and optoelectronic uses. In particular, the development of ceramics that possess higher purity, strength, and homogeneity is of major industrial interest. Due to their viscous properties, the sol gels are also easily used in the development of thin films from such techniques as dip-coating, spraying, and spin coating [2]. In order for the sol-gel monoliths to be used in industrial applications, subsequent processes like aging, drying, stabilization, and densification must be employed. These processes, in turn, depend upon the morphology and structure of the resultant sol gels. Therefore, fundamental studies of the chemistry and physics during the earliest stages of these sol-gel forming systems are necessary for optimizing sol or gel-forming processes.

Metal alkoxides are popular metal-oxide ceramic precursors because of the purity of the starting materials, the low temperature at which the reactions occur, the ease of the reactions, and their reactivity toward water. Essentially, two governing reactions are involved in the metal alkoxide method: hydrolysis and condensation. The relative rates at which these reactions occur determine the structure and morphology of the gels; therefore, it is necessary to understand the kinetics of hydrolysis and condensation. For experimental purposes, these reactions must be carried out in a non-aqueous environment such as ethyl alcohol, since the transition-metal alkoxides react instantaneously with water to form undesired precipitation products [3]. In order to control this instantaneous precipitation, either the concentration of alkoxide can be very much larger than the concentration of water or a catalyst such as acid or base can be added to retard the hydrolysis and condensation reactions. Therefore, such parameters as

* Author to whom all correspondence should be addressed.

‡ Managed by Lockheed Martin Energy Research Corp. under contract DE-AC05-96OR22464 with the U.S. Department of Energy.

(alkoxide)/(water) ratios, water concentration, pH, and temperature must be investigated to elucidate the early-stage chemistry and physics [4]. In order for the size and morphology to be consistently reproduced, the kinetics of these reactions must be understood in detail, that is, the soluble-species consumption kinetics due to hydrolysis as well as the gelation or aggregation kinetics from condensation.

The level at which metal alkoxides can be used in the fabrication of advanced ceramics remains limited because of the difficulties associated with understanding and control of early-stage reactions and sol-gel formation. Zirconium alkoxide reacts vigorously with water to form either a precipitate or a gel. The chemistry that controls the resultant particle size and morphology often occurs within 1 s. For industrial purposes, the reactivity of these precursors poses a problem that must be simplified. For example, in industrial coating processes the hydrolysis and condensation chemistry must be controlled within this time frame if the deposited film is to meet specified criteria [2]. In the present study, zirconia gels were formed by zirconium *n*-butoxide hydrolysis and OH^- was used as an inhibitor. In previous efforts several problems have been encountered in the elucidation of hydrolysis chemistry of metal alkoxides [5]. First of all, the hydrolysis is very fast and impossible to monitor without the aid of an in situ method at very small reaction times; all products are reported as time-averaged concentrations [6, 7]. Second, since hydrolysis competes with condensation so that there is a simultaneous burst of hydrolyzed monomers as well as condensed products, it is very difficult to accurately determine the hydrolysis rate coefficients, K_H. Finally, the possibility that hydrolysis is reversible has been neglected, based on the assumption that adding enough water ensures complete hydrolysis before significant condensation occurs [8].

Alcoholic solution systems of tetraethoxsilane ($Si(OR)_4$, where $R = C_2H_5$) have been exhaustively studied [9]. In fact, most of the work on metal alkoxides has emphasized these systems. To a lesser extent, titanium alkoxide solutions in alcohol have also been studied. Growth models have been predicted and experimentally verified at long times for both silica and titania systems [10–12]. The reaction kinetics of transition metal alkoxides are orders of magnitude faster than those for the silica system. Whereas in the silica system, kinetics can be studied on a time scale of a minute or an hour, the zirconia and titania systems must be studied on a time scale of a millisecond to second, since these react much more readily with atmospheric water. It is, therefore, necessary that an in situ reaction scheme be employed that allows for analyses to be performed in a millisecond time regime. The method of choice is called *continuous rapid mixing* [13]. Recently, Harris and coworkers have published some results for the hydrolysis and condensation mechanisms of zirconium alkoxides at early stages wherein the inhibitor used was H^+ [14].

In the 1950s, Bradley published a series of papers that dealt with several aspects of group IV metal alkoxides (Ti, Zr, etc.) [15, 16]. However, most of the literature emphasizes the titanium group IV metal alkoxides [17]. Very few studies have been made on the initial stages of the reactions involving the hydrolysis and condensation pathways of zirconium alkoxides. Recently, Kumazawa and co-workers used zirconium tetrabutoxides to prepare ZrO_2 particles by controlled hydrolysis [18]. These researchers studied the same systems as those used in the current study; however, their experiments were for much longer times. They investigated the relationship between particle size, initial zirconium tetrabutoxides, reaction temperature, and reaction time. Nevertheless, experimental results are still lacking in the literature to verify the growth mechanisms that result in zirconia gels rather than particles. Yoldas has studied the properties and parameters that affect zirconium oxides formed by alkoxide hydrolysis and condensation mechanisms [4]. Singhal and coworkers have recently investigated the zirconia gelation systems using an inorganic acid as an inhibitor to hydrolysis [19]. A few spectroscopic studies on the group IV metal alkoxides with an emphasis on the structural aspects of these species have been reported, but no data were obtained at the earliest stages of hydrolysis and condensation [20].

Guilment and coworkers suggested that as the molar ratio of (water)/(alkoxide) increased, the tendency for the reactants to form a precipitate would be greater [20]. There is, in fact, a more complete removal of -OR groups as this ratio increases. One reason for instaneous precipitation is that at such high hydrolysis ratios, the -OR groups are nearly completely removed from the molecular structure. Solubility in ethanol will require the presence of a few residual OR groups in solution that have not been completely hydrolyzed [3]. In general, localized condensation occurs once the water/alkoxide ratio exceeds a critical concentration. Consequently, phase separation will occur, as evidenced by the appearance of a milk-colored solution. The introduction of base or acid into the systems helps to prevent the localized condensations and thus serves to maintain a clear solution at the earliest stages. Smit has stated that as this hydrolysis ratio decreases, smaller amount of the zirconium alkoxides will become hydroxolated [21].

Data have not been published for the earliest stages of hydrolysis and condensation of zirconium butoxides using base as an inhibitor. One of the chief objectives of the present study was to provide a database as well as a preliminary mechanism for the nucleation and growth of alkoxide processes. With the aid of a method developed in our research group, it is now possible to study the early stages of these reactions. The rapid-mixing technique has been successfully used for systems that are catalyzed by H^+ [14, 22], but not for systems in which base is used as the catalyst. This paper reports the data obtained and conclusions that were drawn in our study of zirconium butoxides in a weak base.

For the purpose of this study, the synthesis of oxide gels from zirconium alkoxide precursors was investigated by the rapid flow-mixing technique coupled with FTIR and SAXS analyses. The main thrust was to experimentally determine the hydrolysis, condensation, and gelation kinetic parameters of zirconium butoxides in the presence of OH^-.

2. Experimental methods

2.1. Materials

Technical-grade zirconium tetrabutoxide in 80% butanol was obtained from Aldrich Chemical Company. Also, 200 proof reagent-grade absolute ethanol from Aaper Alcohol and Chemical Company, and volumetric-titration-grade tetramethyl ammonium hydroxide ($(CH_3)_4NH_4OH$) from Aldrich were used. All the water in the experiments was doubly deionized, so that the conductivity measured below 18 mmho·cm^{-1}. All solvents were used as received; no further modifications or purifications were performed. All glassware was cleaned by soaking in 2 M H_2SO_4, followed by thorough rinsing with distilled water and drying in air at 180°C. Before using, the glassware was rinsed with dry ethanol. The reactant concentrations used in the studies are shown in Table I. Since the ethanol and alkoxides readily absorb moisture from the air, special care was taken to prevent excess exposure of the solutions to the atmosphere.

2.2. Continuous rapid-mixing apparatus

The extreme lability of zirconium alkoxide systems toward hydrolysis made it necessary to study these reactions using a continuous-rapid-mixing technique (see schematic in Fig. 1) so that information could be gained about the earliest stages of hydrolysis and condensation.

An Ismatec peristaltic pump (MV-GE) was used to perform the rapid mixing experiments. Silicon tubing was used in the pump to ensure sufficient pressure to cause flow. However, Teflon tubing (1/16 in. ID) was used whenever possible to minimize potential reactions that might occur between the solution and the tube wall. The rapid-mixing, continuous-flow experiments were performed by maintaining an equal flow rate of zirconium butoxide/ethanol and H_2O/base/ethanol reactants into a mixing tee (1/32 in. ID). The reaction starts at the mixing tee, where the two solvent streams are mixed in a 1:1 fashion. The concentrations of the stock solutions are immediately diminished by 50% once they mix in the tee. For example, the concentrations of the stock solutions of 0.2 M Zr butoxides and 2.2 M H_2O/0.01 M OH^- would instantly become 0.1 M and 1.1 M/0.005 M, respectively. The maximum achievable volumetric flow rate with the pump was $Q = 2.9$ cm^3/s; however, all experiments were performed at a flow rate of 1.5–1.8 cm^3/s, since the silicon tubing would frequently rupture at the highest flow rate, due to the rapid material breakdown from the pump heads. The volumetric flow rate in a peristaltic pump was found to be essentially independent of the length of tubing used.

Different reaction times were probed by changing the length of tubing between the mixing tee and the sample detector. The time of reaction is defined in these experiments as the time of residence of the fluid in the reactor (i.e., the section from mixing tee to the detector): $\tau = V/Q$, where V is the volume of reactor (cm^3) and Q is the volumetric flow rate (cm^3/s) so that the units of τ are given in seconds.

Since all experiments were performed at the same flow rates, it was assumed that the calculated Reynolds number was a good indication that thorough mixing is obtained in this turbulent regime. The Reynolds number was calculated using ethanol as the basis since the volume of ethanol is so much larger than that of either water or alkoxide. The calculated Reynolds number was $N_{Re} > 2900$ for all experiments. The transition regime from laminar to turbulent is about 2000–3000 for circular pipes [23]. This ensured that mixing was almost in the turbulent regime so that radial gradients of temperature, concentration, and flow were negligible. Once the volumes of the fittings, mixing tee, and appropriate flow cell were measured, a least volume was calculated as that volume which values would occur if the

TABLE I Reactant concentrations (mol/L) used in the study

Experiment	[$Zr(OC_4H_9)_4$] (M)	[H_2O] (M)	[OH^-] (M)
A	0.1	1.1	0.01
B	0.1	1.1	0.005
C	0.1	1.1	0.0025
D	0.1	0.55	0.01
E	0.1	0.55	0.55
F	0.1	0.55	0.0025

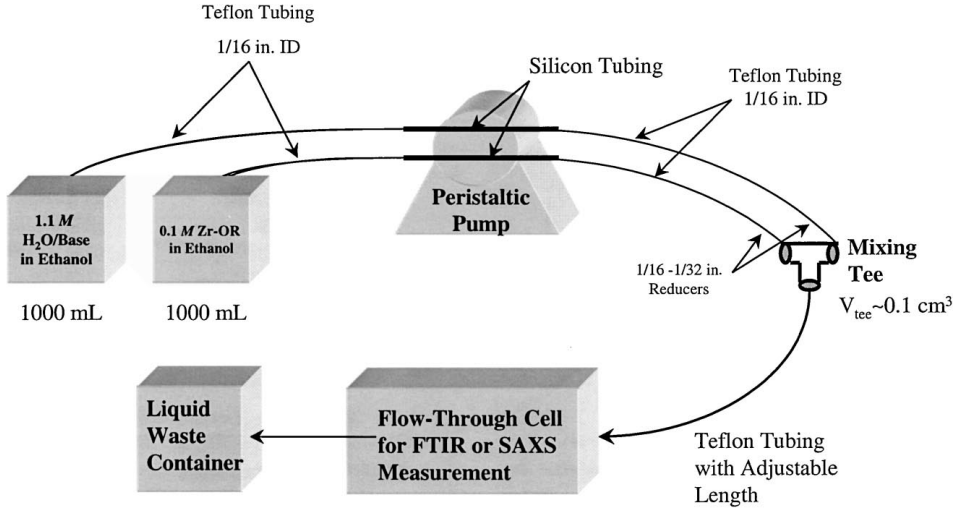

Figure 1 Schematic setup for flow-through rapid-mixing experiments.

point of observation were as close as is mechanically possible. From this, the best time would be calculated as the shortest residence time possible, $T_{best} = V_{best}/Q$. The points of observation for this study were either a manufactured flow-through cell from Spectra-Tech or a homemade flattened quartz capillary.

2.3. FTIR analysis

Infrared spectra can be used as "fingerprints" both to identify and to determine the concentration of a particular species. By monitoring the relative detected intensity at the characteristic fingerprint regions, it is possible to determine the concentration of a given species in the sample of interest. All FTIR experiments were performed on a Nicolet 560 Spectrophotometer (with a liquid nitrogen–cooled MCT detector at a spectral resolution of 8 cm^{-1}) to determine the relative concentrations of the reactant species (i.e., water and -OR in zirconium tetrabutoxide) as the reaction progressed. The spectrophotometer was controlled with OMNIC software provided by Nicolet on a PC computer with a Windows 3.1 platform.

The first step in determining the concentration of the species of interest was establishing a standard calibration curve for each (1685–1619 cm^{-1} for water and 1180–1120 cm^{-1} for Zr-O-R). The typical standard calibration curves (concentrations vs. peak areas) for these reactants are straight lines. It was determined that the 34°C and the 23°C standard curves had about the same slope for the linearly regressed data, whereas the 10°C standard curves had a lower linearly regressed slope. This phenomenon was due to the fact that the colder temperatures slowed down the rotational and vibrational movements of the molecules, thus, reducing the measured intensity. An experimental technique known as solvent extraction was successful in resolving the associated fingerprint regions. This technique is extremely useful for organic solvents since they demonstrate very high absorption. The background is assumed to be the sample cell containing ethanol, which is then subtracted from all sample spectra. In order to further eliminate any background interference from either temperature or fluid flow phenomena, the individual backgrounds were taken at the same temperature and flow rates as the experimental conditions. Using the linear regression lines from the standard curves, the concentrations were calculated as a function of the integrated areas for the fingerprint regions. The initial concentration of the species at $t = 0$, $[H_2O]_0$ and $[Zr\text{-}O\text{-}R]_0$, were taken to be the extrapolated values from the standard curves whenever only the reactants of interest were present in the reactor.

In order to reduce the risk of affecting the spectra with moisture, the sample chamber was opened as little as possible, by performing multiple experiments with different concentrations (A through F) at a given reactor volume before changing the tubing. Between each set of experiments, the tubing was thoroughly rinsed with ethanol for at least 30 s so that the next experiment would not be contaminated by the preceding one. A reference standard of 1.5 μm polystyrene film with a known spectrum was used to determine the effect of atmosphere on the output. Once this spectrum was obtained, it was matched against a library of spectra found in the accompanying software package for the spectrophotometer. For all experiments, the statistical library search matched the polystyrene reference with 95% accuracy.

The cell windows were made from ZnSe, a material that has very negligible absorbance in the mid-infrared regions (4000–400 cm^{-1}). The window had a radius of 18 mm and a width of 2 mm. In order to accommodate flow, one window was placed upon the other separated by a grooved aluminum or Teflon spacer. The groove helped to minimize the volume between the windows to ensure a continuous reaction pathway and to minimize backmixing in the reactor. The typical slit width between the windows was 100 μm, which was found to be the optimum width. At smaller distances, pressure buildup occurred, causing leakage. At greater distances, the spectral distinction of alkoxides diminished due to difficulties in discriminating solvent background from a sample. However, at the optimum width, the background noise due to the solvent was virtually eliminated via the solvent subtraction technique.

Different reaction temperatures were also studied so that activation energies and rate constants could be determined. For experiments wherein the temperature was not ambient, thermocouples were used to monitor the process conditions at the inlet and outlet of the flow-through cell. That is, one thermocouple was placed immediately before the mixing tee and the other was placed immediately after the sample cell. The average of the two associated temperatures was taken to be the reaction temperature. The temperature sources that were used in the experiments were water baths maintained at 5°C and 40°C. The actual experimental temperatures were 10, 23, and 34°C, respectively. To ensure that localized temperature gradients were minimized, the reaction flasks were incubated in the baths for at least 30 min. The temperature drop between the two thermocouples was much smaller than that between the water bath and the first thermocouple. In other words, heat loss was due more to surface area convection to the atmosphere than to the relative heats of reaction that may occur.

2.4. SAXS analysis

Small-angle X-ray scattering (SAXS) was used to establish a preliminary data base of the relative size of primary particles as well as structural transitions during the condensation reactions. SAXS experiments were conducted on the 10-m SAXS instrument at Oak Ridge National Laboratory [24]. The X-ray source was a 12-kW Rigaku rotating-anode generator operated at 40 kV and 100 mA with a copper target and a graphite crystal monochromator. A pinhole collimator and a 20×20 cm^2 dimensional position-sensitive counter of 64×64 channels were also used. In order to absorb X-rays close to the zero scattering angle so that the detector was not burned, a 1-cm diam lead beam stop was used. The sample-to-detector distance was set at

either 1.069 or 5.069 m. The sample holder, which was constructed from aluminum, was used to hold a homemade flattened glass or quartz capillary which was used as a flow-through reactor. The flattened capillaries were made by melting 2.0-mm-diam capillaries between two graphite blocks that contained fixed grooves at ~600°C for 1 h. Once these capillaries were flattened, they were carefully glued in the aluminum holder with Du Pont® 2-Ton epoxy and left to dry.

Several preliminary corrections were performed before collecting data. The sample scattering was corrected for detector sensitivity, dark current, and background solvent. The sensitivity run was performed by closing the gate valve between the X-ray source and the sample chamber and inserting ^{55}Fe, an isotope that emits X-rays, into the sample holder. Collection time on the detector using the ^{55}Fe as the X-ray source lasted about 3–4 h. In order to determine the relative effect of scatterings from cosmic sources and other substantial radiation sources, a dark-current correction was also performed. To measure the dark current, both gate valves were closed so that the detector would only detect cosmic radiation. Collection time on the dark current usually took about 1–2 h. The third correction was to account for background solvent. Although the other two corrections could be performed at any time during the experiments, it was necessary to correct for background before data collection, because the scattering was dependent on both the solvent and the local morphologies of the flow-through cell. Therefore, all solvent corrections were measured in the same cell as that in which the actual data were measured. It was also necessary to measure the transmission coefficient of the scattering materials so that the intensity would be measured with respect to this value:

$$T_m = \frac{(I_{gcs} - I_{dc}) - 0.686\,(I_s - I_{dc})}{(I_{gc} - I_{dc}) - 0.686\,(I_{mt} - I_{dc})},$$

where I_{gcs} is the measured intensity of glassy carbon and sample (glassy carbon being an automated filter that has a characteristic scattering intensity), I_{dc} is the number of counts from the dark current, I_s is the sample scattering intensity, I_{gc} is the measured intensity from glassy carbon alone, and I_{mt} is the measured count rate, in hertz, of the empty beam. From the transmission, the thickness of the capillary was calculated; typical values were found to be 0.8–1.1 mm.

Whenever an incident X-ray beam bombards a particle, the angular dependence of the scattered intensity is measured. A small-angle-scattering curve from a typical dilute macromolecular solution includes Guinier, Porod, and Bragg regions [25, 26]. The Bragg region is characterized by large scattering angles; information from this region is useful in studying interatomic spacings. The Guinier region is characterized by small scattering angles. The Porod region occurs at intermediate angles. The Guinier and Porod regions were the two areas of interest for the studies reported here.

The theory of SAXS has been worked out in detail by Guinier [27]. With SAXS, it is possible to investigate structures on length scales from ~5 to 1000 Å. Small angle X-ray scattering arises from the electron-density differences between a particle and the medium in which the particle is embedded. The scattering depends on the number of particles, the electron contrast between particle and the medium, and the size of the particles themselves,

$$I(q) = I_e(q) N_p (\Delta\rho v)^2 \exp\left(-q^2 R_g^2/3\right),$$

where v is the volume of the particle; N_p is the number of particles per unit volume; R_g is the radius of gyration; I_e is the scattering from a single electron; $\Delta\rho$ is the electron density difference between the particle and the medium; and q is the scattered wave vector, $q = (4\pi/\lambda)\sin\theta$, where 2θ is the scattering angle and λ is the wavelength of the incident X-rays. The wavelength of the X-ray was 1.54 Å, which is considerably smaller than the size of the particles being detected.

The radius of gyration (R_g) is defined as the weight-average radius of the particle. The R_g values can be found from the scattering data by means of a Guinier plot. For data in the range $qR_g < \sim 1.3$, plotting ln I vs. q^2 gives a straight line with a slope of $-R_g^2/3$. The zero-angle scattering intensity, $I(0)$, which is obtained by extrapolation of Guinier's law to $q = 0$, gives useful information about the number of particles and electrons in each particle: $I(0) = I_e(0) N_p (\Delta\rho v)^2$. The above scattering formula holds primarily for monodisperse systems; however, curvature in the Guinier plot is observed for systems with a wide range of polydispersity. Guinier data exhibit a bias toward the largest particle size since these bulkier species dominate the data at low q, whereas smaller particles dominate the data at high q. Most of the relevant information about the structure of the particle occurs for $0.1 < qA < 20$, where A is defined as the diameter of the particle, or the largest distance that can be scanned between two discrete points in a particle. The inequalities represent the extremes as either high or low q values. A compromise that is commonly used in dealing with this bias is referred to as the resolution criterion [28]. Although R_g is a parameter that intuitively relates the size of a particle to its spatial extensions, the radius of gyration is useful in characterizing certain geometries. For example, the radius of a sphere is given by $R_s = \sqrt{(5/3)}R_g$, whereas long rods are characterized by $L \simeq \sqrt{12}R_g$.

Scattering at intermediate angles ($R_g \gg q^{-1} \gg A$) can be characterized by the Porod Law, in which the data can be modeled as a power law, $I \propto q^{-D_f}$, where $-D_f$ is the slope of the regressed line from the $\log I \sim \log q$ plot. Whenever $0 \leq D_f \leq 3$, the system is characterized by mass fractals, D_f [29]. The Porod region is useful in monitoring the structural stages that occur during the polymeric gelation process. From fractal dimension analyses, it is possible to predict the structure as well as the growth mechanisms for the metal alkoxide polymeric clusters and species [9].

Three main issues were investigated in this study by using the SAXS technique: size (R_g, radius of gyration), structure (D_f, fractal dimension), and growth kinetics (dR_g/dt) of the condensation products that are formed during the hydrolytic condensation of metal alkoxides.

The primary importance of R_g is to establish the initial size of the metal alkoxide in solution. It is then possible to know whether the metal alkoxide exists as a monomer, trimer, tetramer, or some other structure. The shape of an overall kinetic curve is a function of the overall interaction potentials between the aggregating clusters and the rate of the condensation reaction.

2.5. Hydrolytic chemistry of alkoxides

The chemistry involved in the sol-gel process is based on inorganic polymerization [3, 9, 15]. The precursors for these polymers are generally metalloorganic compounds such as the metal alkoxides, $M(OR)_n$ [7]. Starting from molecular precursors, an oxide network is obtained via a series of hydroxylation and condensation reactions:

$$\text{hydrolysis: M-OR} + \text{H}_2\text{O} \rightleftarrows \text{M-OH} + \text{ROH},$$
$$\text{condensation: M-OH} + \text{ROM} \rightleftarrows \text{MOM} + \text{ROH}$$
$$\text{or M-OH} + \text{HOM} \rightleftarrows \text{MOM} + \text{H}_2\text{O}$$

where R represents an alkyl group and M signifies the metal of interest. For the systems of interest in this study, M will be zirconium and -R will be a butyl group, $-C_4H_9$. Barringer has proposed that hydrolysis and condensation are not simultaneous reactions, and therefore not competitive, and that the mechanisms can be analyzed in a mechanistic approach [17]. That is, hydrolysis and condensation are essentially a series of initiation and propagation steps, wherein hydrolysis is the initiation step followed by condensation. According to Barringer, the hydrolysis reaction is the rate-limiting step, wherein three of the four -OR groups are readily eliminated. The fourth alkoxy group is often very difficult to remove, and it sometimes is never removed due to steric hindrance as well as solvent effects.

Transition-metal alkoxides are fairly electropositive, and their oxidation states are usually smaller than those of other metal alkoxides [15]. The result is that they will readily react with nucleophilic agents so as to increase their coordination [3]. During hydrolysis, a hydroxyl ion becomes attached to the metal atom, thus leading to the formation of hydroxylated M-OH groups. Depending on the amount of water and catalyst present, hydrolysis may or may not go to completion. It is possible that only a few of the -OR ligands will be replaced by -OH groups so that the metal is only partially hydrolyzed. Two partially hydrolyzed molecules can link together in a condensation reaction. Condensation is a process that liberates a small molecule such as water or alcohol en route to the formation of polymer [9].

There are essentially three mechanisms for condensation by hydrolytic reactions of alkoxides. *Olation* is a condensation process in which a hydroxy bridge is formed between two metal centers, Zr-OH-Zr. This is a nucleophilic substitution (Sn) reaction wherein the hydroxy group is the nucleophile and H2O is the "leaving" group. An Sn reaction is one in which a "nucleus-loving" reagent (one that is electron deficient) attacks an atom such that a substitution occurs and there is a departing (or leaving) group so that the overall charge on the species is conserved [30]. Consequently, the rate at which olation occurs is related to the lability of the aquo ligand ($-OH_2$), which depends on size, electronegativity, and the electronic configuration of M. *Alcoxolation* is a condensation reaction in which an oxo bridge, M-O-M, is formed between two metal centers via nucleophile addition and the leaving group is R-OH [4]. Nucleophilic addition occurs whenever an electron-rich nucleophile attacks an electron-deficient area of a molecule. After coordination and charge transfer, a leaving group will exit to accomodate the addition. The third condensation mechanism is a water-elimination mechanism (*oxolation*) during the formation of an oxo-bridge, M-O-M. Livage *et al.* have proposed that alcoxolation is the predominant mechanism for the condensation process [3]. Whenever the preferred coordination of the metal is satisfied, the condensation will proceed via an Sn reaction; whenever the preferred coordination is not satisfied, it will proceed via a nucleophilic addition (An) reaction. An overall hydrolytic polycondensation that takes into account the variability of the alkoxide (M-OR), hydroxide (M-OH), and oxide (M-O-M) has been established by Day *et al.* [14, 31],

$$n\text{M(OR)}_4 + (2n + (x - y)/2)\text{H}_2\text{O} \rightarrow \text{MnO}_{(2n-(x+y)/2)}(\text{OH})_x(\text{OR})_y + (4n - y)\text{ROH},$$

where n is the number of zirconium atoms in the polymer and x and y are the numbers of OH- and OR-groups in the molecule [31]. Hydrolysis, condensation, and alcoholysis can each be described by the following three-step process [3]:

1. nucleophilic addition of negatively charged OH groups to positively charged metal atom M.
2. proton transfer within the transition state complex from the entering ligand (XOH) towards a negatively charged oxygen of an adjacent alkoxy group.
3. departure of the protonated (R-OH) species.

From these three steps, it is clear that the reactions depend on the relative partial charge distribution. The following conditions must, therefore, be fulfilled: $\delta(\text{M}) > 0$, $\delta(\text{OR}) < \delta(\text{H})$, and $\delta(\text{ROH}) > 0$. The rate-limiting step for the overall reaction occurs whenever these criteria are not fulfilled. It is necessary that the partial charge of the various species in the reactants, transition-state complexes, and intermediate products be computed [11]. In order to elucidate the difficulties of these reactions, Livage proposed a model called the Partial Charge Model (PCM). The PCM describes the chemistry of each of these reactions in terms of the chemical moities that are present at any given time and the localized charges associated with them [3]. PCM also allows one to qualitatively predict the reaction scheme for the hydrolysis and condensation reactions based on the electronegativity of the attacking and leaving groups.

Since water has a very high dielectric constant, it contributes to the dissociation of the ionic species; it behaves as a sigma donor, thus acting as a good nucleophile. The driving forces for these nucleophilic reactions to take place are the low electronegativity of the metal organic precursors as well as the desire for the d^0 transition metals to increase their coordination numbers by accepting lone pairs of electrons from the nucleophilic ligands. The basis for the model is the principle of "electronegativity equalization" [32] which states that "when atoms of different electronegativity combine, they adjust to the same intermediate electronegativity in the compound." This model has been used to predict the relative rates of hydrolysis and helps to clarify why the partial charge of $\delta(Zr(OR)_4) > \delta(Ti(OR)_4) > \delta(Si(OR)_4)$. The most rapid hydrolysis rates in this series are those of zirconium, which is the most electropositive of the metal ligands.

The model has also been used to study the effects of acid and base catalyst on the hydrolysis and condensation reactions. The theoretical predictions of polymeric growth from the PCM agree with the experimental results. The model suggests that H^+-catalyzed condensation processes are directed toward the end of a chain rather than the middle, whereas OH^--catalyzed condensation is directed toward the middle of a chain. The net result of these two mechanisms is that either more extended, less highly branched polymers or more compact, highly branched polymers will be formed, respectively [9].

2.6. Cluster/particle growth during condensation

The number of bonds that a monomer can form is called the functionality, f. Whenever $f > 2$, polymers may form three-dimensional cross linked structures [9]. The polymerization of zirconium and titanium alkoxides, for example, may lead to this complex branching since the fully hydrolyzed monomer, ($M(OH)_4$), is tetrafunctional. However, under certain reaction conditions such as variations in water concentration and different acid or base concentrations, fewer than four ligands will be capable of condensation. This implies that little branching will occur. To further elucidate the trends for either cross-linked or linear polymers, experimental work must be performed using SAXS. It is readily verified that the cumulative ratio, $([H_2O]_0 - [H_2O]/(4([M\text{-}OR]_0 - [M\text{-}OR]))$, is equal to unity whenever there is hydrolysis without condensation [14]. The symbol $[\ ]_0$ denotes the initial concentration of either water or the M-OR ligand. Whenever condensation is also occurring, the cumulative ratio is less than unity and approaches 0.5 when condensation is much more rapid than hydrolysis. Depending on factors such as pH, reagent concentration, and temperature, the hydrolysis and condensation reactions can result in the formation of gels, flocculated precipitates, or powders.

The aggregation or growth mechanisms for colloidal particles are rooted in the theory of classical colloidal stability. They are a function of the total interaction potential, V_t. The foundational theory that accounts for the competitive forces involved in the total potential is the DLVO (Derjaguin, Lanadau, Verwey, and Overbeek) theory. The DLVO theory describes the stability of colloidal particles as a function of the overall forces that are present in a system: the attractive van der Waals, the electrostatic repulsive, and the solvation interaction potential [10]. This competition determines the stability or instability of colloidal systems [33–36].

Several aggregation models presently exist in the literature for describing gelation phenomena. Since condensation is not a reversible process, bonds form randomly. Consequently, polymer formation is governed by Brownian diffusion as well as interparticle and intermolecular forces. Fractal structures are formed whenever a monomer forms bonds at random. Most of our current knowledge about fractal aggregation exists in computer simulation models, since it is nearly impossible to experimentally isolate the associated mechanisms with the clarity that computer simulations yield [29]. Some of the aggregation processes are described by the Witten and Sander model, which is simply referred to as the diffusion-limited aggregation (DLA) [37]; the Percolation model, wherein it is assumed that the reactivity of all the functional groups on a monomer is equally probable and that bonds form between polymers and not within them [9]; and the reaction-limited-aggregation model (RLA), where growth occurs strictly by condensation of monomers with clusters or by condensation of clusters with other clusters [38]. In DLA, particles traverse by random "walks" and irreversibly collide with immobile clusters. To this point, all DLA computer simulations have either admitted the effect of Brownian motion or the effect of chemical processes that govern the motion of the polymeric species. In most DLA-characterized systems, the diffusing polymers grow according to their sticking probability. Recently, results have been reported wherein the aggregative growth was due to both DLA and RLA [39]. It is not the focus of the present study, however, to simulate any of these growth processes with computer models, but to use the results of current models to describe the growth that occurs during gelation.

The main focus of this paper is to experimentally determine parameters that affect the hydrolysis, condensation, and gelation kinetics. By combining the results of these experimental analyses, it may be possible to establish an overall kinetic model that will account for the soluble-species reaction kinetics as well as the kinetics of aggregation due to the condensation and diffusion processes.

3. Results and discussion

3.1. Hydrolysis and condensation processes

A weak base, tetramethyl ammonium hydroxide, was used as the catalyst for reactions in solutions of zirconium butoxide in ethanol.

Our data supports that hydrolysis and condensation are not reversible reactions [17]; instead, they are overlapping or occur simultaneously. That is, hydrolysis does not go to completion before condensation begins. Nevertheless, the dominant mechanism in the earliest stages is indeed hydrolysis. In fact, most of the hydrolysis readily occurs within 1 s. It is evidenced, too, from the experimental data that the early stages of condensation begin to occur within this time scale. Therefore,

this was the primary time frame of interest in the present study for quantitative analysis, although several data points were collected for longer times. To elucidate the physics and chemistry for this region implies that one can control the resultant morphology of the product gels or powders of interest. The earliest time that was achieved was 100 ms.

Hydrolysis and condensation are facile reactions in the presence of water, because of their low electronegativity and their desire to increase coordination by accepting electrons to occupy the outer d^0 shells. These two factors make them susceptible to nucleophilic attack from hydroxo groups. Upon the addition of a strong base, the hydrolysis of metal alkoxide is slowed down significantly. That is, the hydroxo group behaves as an inhibitor to hydrolysis. Bases that do not strongly dissociate into OH^- groups do very little to retard the reaction; in this case, hydrolysis would proceed as if no inhibitor were present. For example, a few attempts were initially made to perform the experiments in the present study with ammonium hydroxide. It was discovered that inhomogeneous precipitation occurred almost immediately, making in situ measurements by FTIR or SAXS nearly impossible with this base. Eventually, tetramethyl ammonium hydroxide was used as the base since it has a very high dissociation constant. Although much of the hydrolysis is completed within 1 s, condensation continues for minutes, hours, or days depending on the (OH^-). Inhibitor concentrations were selected for this study that yielded powders and gels. However, due to experimental limitations, analytical techniques were used only on the systems that formed gels. Instantaneous precipitation was used as a guideline for the amount of base that must be added so that it would be possible to perform the experiments.

3.2. FTIR results

Fig. 2 is an example of solvent-subtracted spectrum for 0.1 M Zr, 0.01 M OH^-, and 1.1 M H_2O taken at 100 ms and 25°C. Spectra such as these were used to monitor the concentrations of both water and alkoxide as the reaction progressed. In all cases, A–F (where data sets A through F are described in Table I), it was observed that the intensity of the Zr-O-R area (∼1120–1180 cm^{-1}), decreased significantly within 1 s, whereas the intensity of the water region (1620–1660 cm^{-1}) either changed very little or actually increased in size after the initial concentration decay. Cases A–C were performed at three different reaction temperatures 10, 23, and 34°C, whereas Cases D, E and F were performed at laboratory room temperature, 23°C. Fig. 3a–f show the percentage of Zr-O-R groups that remain as the hydrolytic condensation proceeds for the different experimental conditions. In Fig. 4a–f, the percentage of water is graphically illustrated for the appropriately labeled reaction conditions. The effects that the OH^- groups have on the rate of Zr-OR at fixed temperatures (10, 23, and 34°C) are seen in Fig. 5a–c.

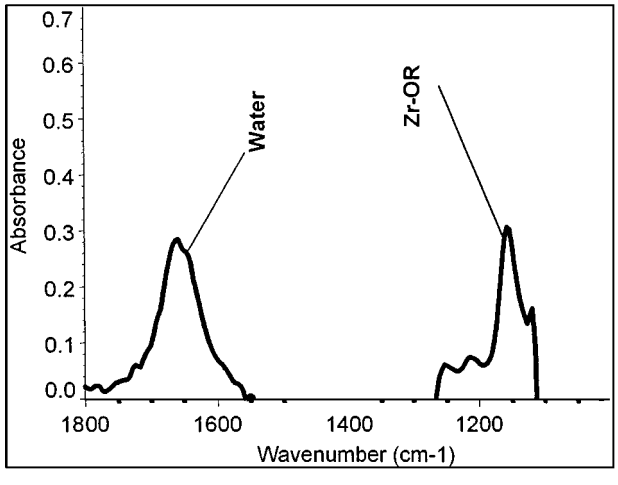

Figure 2 Solvent-subtracted FTIR spectrum during a typical reaction.

Changing the temperature was important in these experiments to qualitatively and quantitatively observe the kinetic phenomena. Fig. 3a–c, along with Table II demonstrate how temperature affects the rate and extent of the hydrolysis reactions. From qualitative observation of the data in these figures, as well as from regression analysis (where r^2 was typically around 0.5 to 0.6), it is easily seen that the overall kinetics do not follow a first–order exponential decay since the first data point at 100 ms is so dramtic with respect to the remaining data points. Fig. 6a–c are examples of the difficulty involved in fitting an overall hydrolysis model for the first 3 s of reaction. These least–squares mathematical fits for the overall hydrolysis scheme were performed using an inverse exponential model, $r_{ZrOR} = 1/(K_H t^n)$. Although this model fits very well mathematically, very little quantitative information can be obtained from it. For example, at time zero the model goes to infinity. Also, the units on the predicted hydrolysis rate constants, K_H,

TABLE II Effect of temperature on [Zr-OR], where $[Zr\text{-}OR]_0$ = 0.4 M

Data set	Temp. (°C)	[Zr-OR] (M) at 100 ms	[Zr-OR] (M) at 300 ms	[Zr-OR] (M) at 1 s	[Zr-OR] (M) at 3 s
	10	0.188	0.168	0.12	0.108
A	23	0.144	0.132	0.1	0.092
	34	0.126	0.108	0.084	0.082
	10	0.3	0.18	0.092	0.068
B	23	0.2	0.152	0.06	0.052
	34	0.144	0.084	0.044	0.036
	10	0.128	0.116	0.088	0.076
C	23	0.108	0.064	0.04	0.04
	34	0.092	0.056	0.028	0.023

TABLE III Parameters for rate expressions using inverse exponential decay model

Data set	Temp. (°C)	K_H (arbitrary)	Order (n)
	10	2.158	0.200
A	23	2.301	0.200
	34	2.469	0.200
	10	2.132	0.202
B	23	2.545	0.260
	34	3.092	0.335
	10	2.486	0.225
C	23	3.195	0.339
	34	3.489	0.384

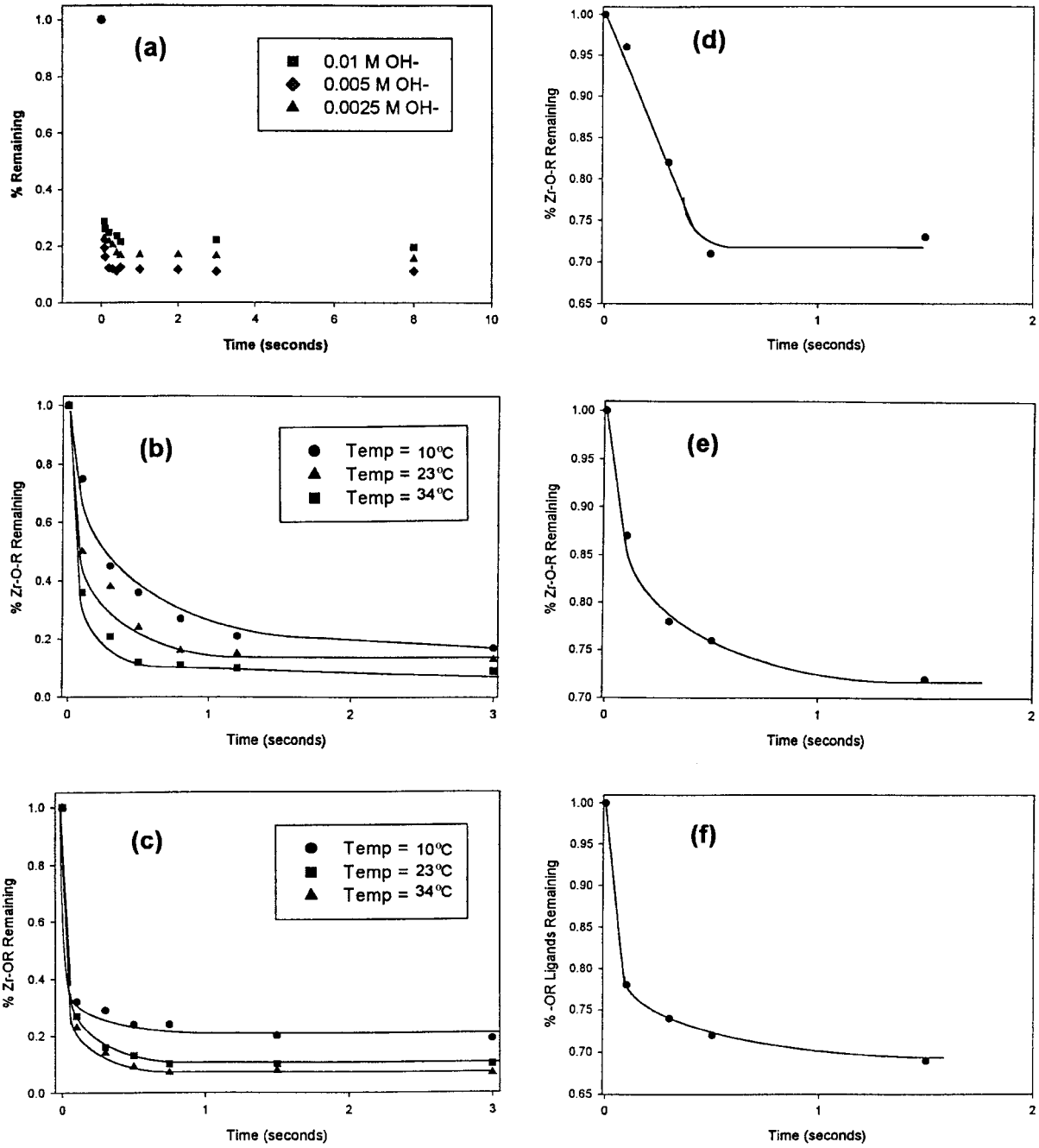

Figure 3 Zr-OR consumption kinetics at various experimental conditions: (a) effect of base concentration while [Zr] = 0.1 M and [H_2O] = 1.1 M; (b) B experiments at various temperatures; (c) C experiments at various temperatures; (d) D experiment at 23°C; (e) E experiment at 23°C; (f) F experiment at 23°C.

are extremely difficult to resolve. Difficulty in finding a fitting model with physical meaning illustrates the complexity of these reactions. Table III summarizes the reaction rate parameters that were computed from these models.

In order to quantify the reaction kinetics, it was necessary to change the reaction temperatures. The activation energy was experimentally determined by carrying out the reactions at varying temperatures, namely 10, 23, and 34°C. The equation used to calculate the activation energy E_A values was [40]

$$\ln K_H = \ln B - \left(\frac{E_A}{R}\right)\left(\frac{1}{T}\right),$$

where K_H is the hydrolysis rate constant computed from a first-order fit on the first two data points, B is a constant, R is the universal gas constant (8.314 J/mol·K), and T is the absolute temperature in Kelvin units.

We can see from Fig. 6a–c that these reactions are too complex to fit with a first-order decay for the entire hydrolysis region; however, a reasonable approximation can be made using a first-order decay for the first data points, since this is where the majority of the hydrolysis is completed. Such an approximation can be supported from the literature wherein Barringer proposed that 75% of the hydrolysis is completed within 1 s and the remaining occurs at much longer times [17]. The "transition region" from 0 to 100 ms is where most of the hydrolysis occurs. The overall chemistry can be observed as a scheme where there are several hydrolysis and (as discussed below) condensation steps. Consequently, it is necessary to apply a first-order model to the first two data points, since this is where the hydrolysis

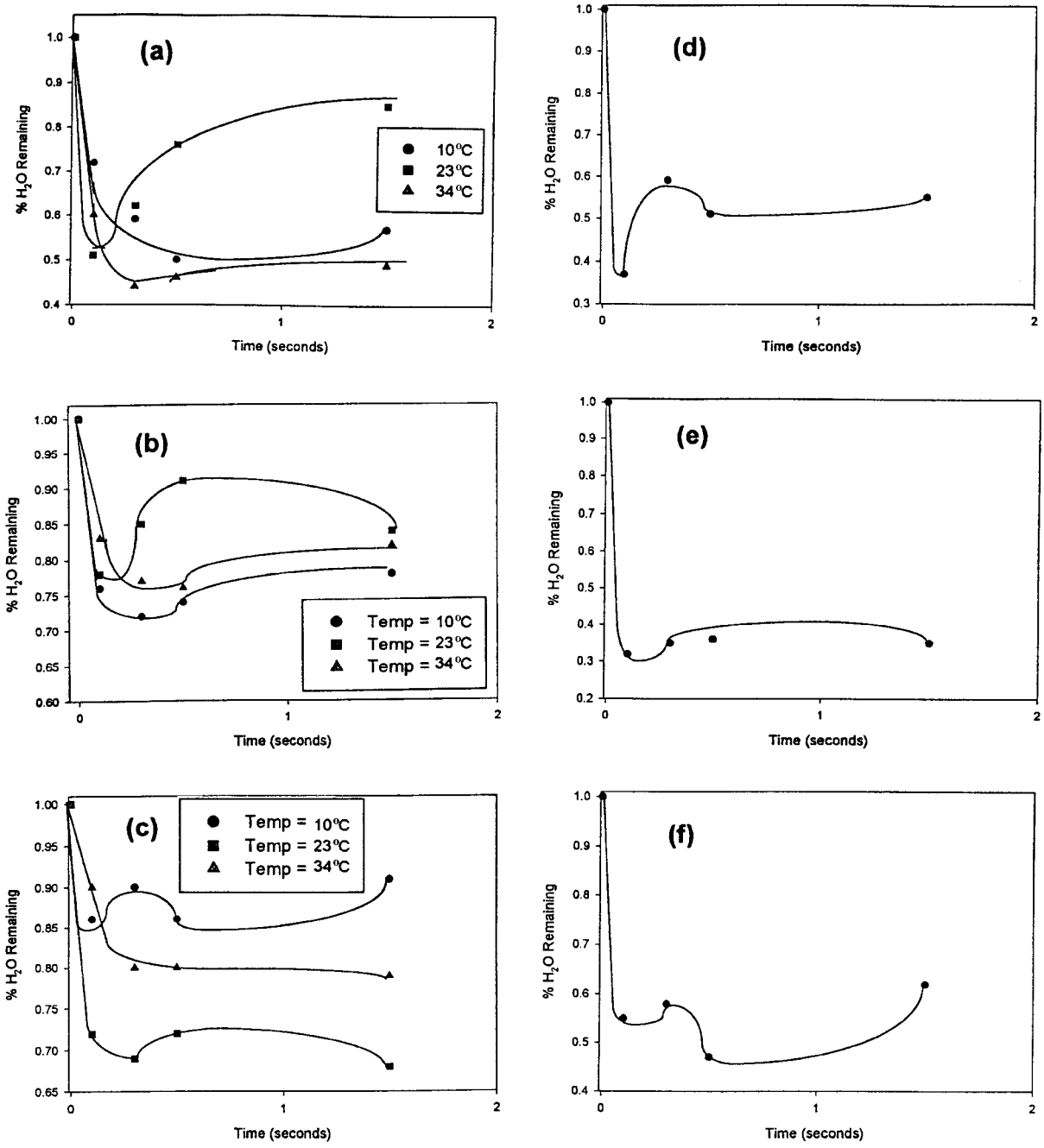

Figure 4 Water consumption kinetics at various experimental conditions: (a) A experiments at 10, 23, and 34°C; (b) B experiments at 10, 23, and 34°C; (c) C experiments at 10, 23, and 34°C; (d) D experiment at 23°C; (e) E experiment at 23°C; (f) F experiment at 23°C.

proceeds to the point that approximately three of the four -OR groups are replaced. First-order linear regression plots where used to determine these initial slopes so that K_H could be estimated. The hydrolysis reaction rate was modeled as:

$$-r_{ZrOR} \simeq K_H[\text{Zr-O-R}],$$

where units for the rate are given in mol·s^{-1}. The analytical method used for the calculation of the initial rates was a graphical technique, where $[\text{Zr-O-R}] = C_{ZrOR}$ (mol/l) was plotted on the ordinate of a log scale vs. time (seconds) on the abscissa [40]. From the slopes of these plots, the first-order hydrolysis rate constants, K_H, were calculated according to the equation

$$\ln\left(\frac{C_{ZrOR}}{C_{ZrOR}}\right) = -K_H t,$$

which, upon rearranging and converting to a common log scale, gives

$$\log\left(\frac{C_{ZrOR}}{C_{ZrOR_0}}\right) = -K_H \frac{t}{2.313}$$

or

$$K_H = -2.313(\text{slope}), \quad \text{where} \quad \text{slope} = \left(\frac{1}{t}\right) \times \log\left(\frac{C_{ZrOR}}{C_{ZrOR_0}}\right).$$

For all calculations, $[ZrOR]_0$ was 0.4 M. Table IV summarizes the values of K_H and E_A that were calculated from the experimental FTIR data for the 0- to 100-ms time regime. As predicted from classical chemical

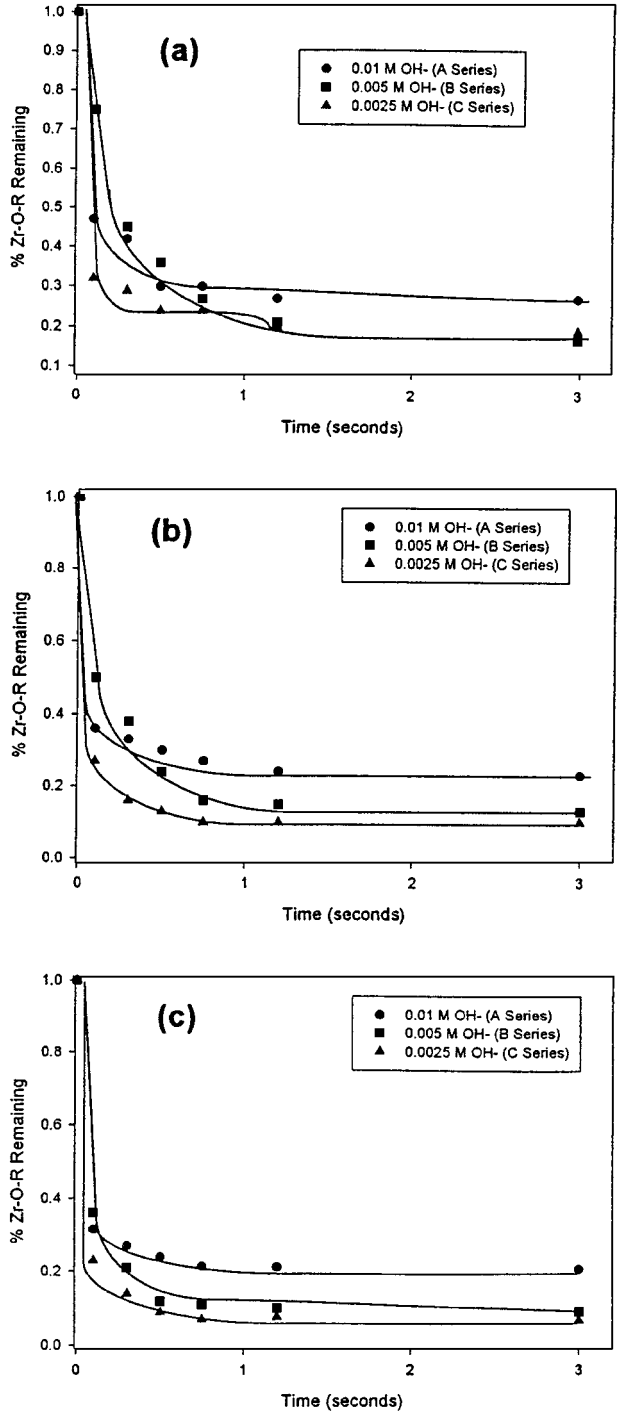

Figure 5 Effect of base concentration on the Zr-OR consumption at reaction temperature of (a) 10°C, (b) 23°C, and (c) 34°C.

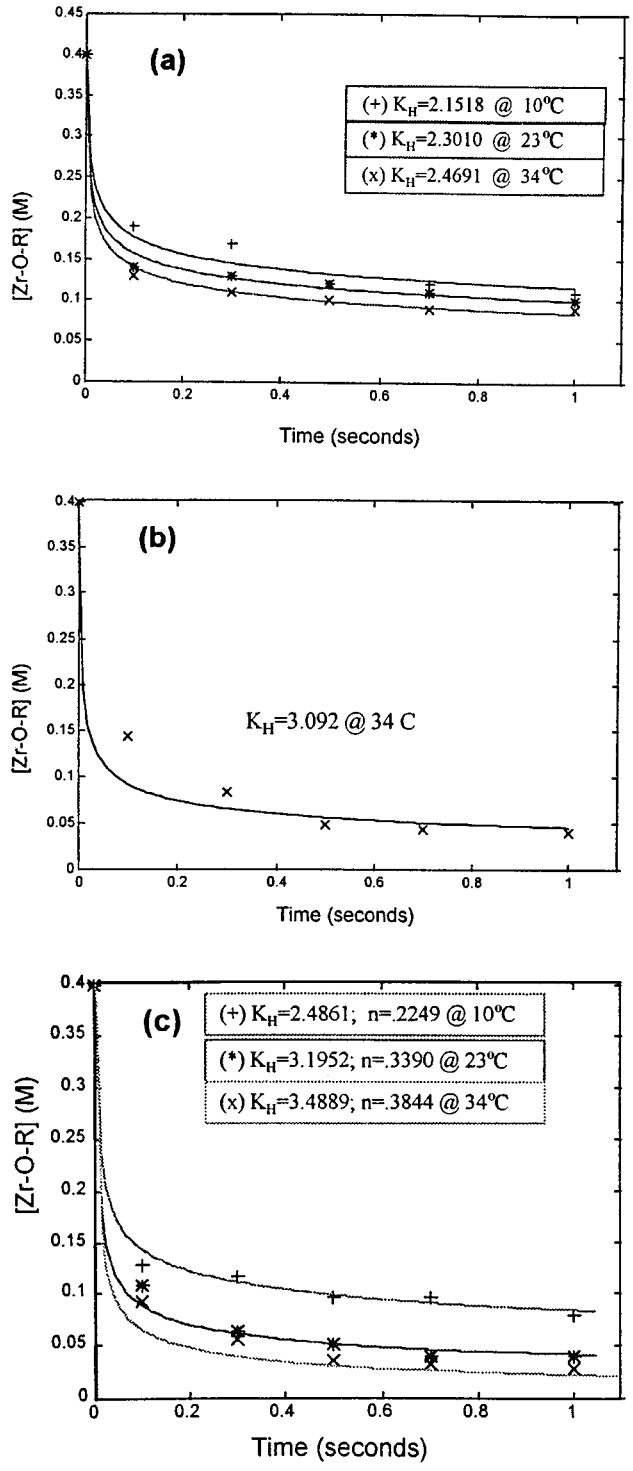

Figure 6 Two-parameter model ($R_{\mathrm{ZrOR}} = 1/(K_{\mathrm{H}}t^n)$ fit for the Zr-OR consumption kinetic data with 0.4 M Zr-OR and 1.1 M H_2O: (a) 0.01 M OH^-, $n \sim 0.2$; (b) 0.005 M OH^-, $n \sim 0.335$; (c) 0.0025 M OH^-; n varies with temperature.

reaction kinetics, the trend in these data is that an increase in temperature accelerates the hydrolysis rate. That is, hydrolysis occurs within this region with a rate law that is first order in substrate. As proposed from Barringer, approximately three of four -OR groups are replaced immediately, whereas the remaining groups are hydroxolated at some later time [17]. Depending on the quantities of initial reactants, the hydrolysis may or may not go to completion.

It was initially anticipated that with decreasing base concentration, both Zr-O-R and H_2O consumption rate would increase. It was also expected that this trend would follow for increasing temperature. However, Fig. 3a shows that the trend for hydrolysis conversion does not necessarily follow the order of decreasing (OH^-). The expected trends for temperature change hold within the data sets (in other words, the data agree with classical chemical kinetics in terms of temperature), as does the degree of hydrolysis with decreasing inhibitor concentration; however, these trends do not apply outside the data sets. The activation energy barrier for data set B is actually greater than for data set A, which has more inhibitor present. Furthermore, the calculated K_{H} values are less than those calculated in data set A at the same temperature values. From these

TABLE IV Summary of experimentally determined hydrolysis rate constants, K_H, and activation energies, E_A, using a first-order graphical technique

Data set	Temp. °C	K_H (s^{-1})	E_A (J/mol)
	10	7.54	
A	23	10.21	13.00
	34	11.52	
	10	2.88	
B	23	6.92	41.30
	34	10.9	
	10	11.39	
C	23	13.09	7.78
	34	14.67	
D	23	0.41	N/A
E	23	1.38	N/A
F	23	2.48	N/A

results, it appears that OH^- competes with H_2O for the d^0 orbitals of the Zr-O-R ligands. Unlike a "true" catalyst such as H^+, OH^- increases the nucleophilicity of the reaction media, thus making the mechanisms a lot harder to predict in terms of the detailed chemistry involved. To further understand this phenomenon, it is essential to observe the water conversion data in Fig. 4a–f. In these figures we see an initial burst of water loss due to hydrolysis. After this burst, several things happen to the (H_2O): (a) the water loss continues, (b) there is an increase in water concentration, or (c) the water level achieves a steady-state value. Although it is not possible to decouple hydrolysis and condensation, it is possible to make predictions as to which condensation mechanism describes the data. As already discussed previously, condensation proceeds via alcoxolation or oxolation, wherein an alcoxolation mechanism implies that alcohol is produced and an oxolation mechanism results in the production of water. If water fluctuation did not occur in this study, it would not necessarily imply a mechanism wherein hydrolysis is completed before condensation begins. Instead, it could be concluded that condensation occurs by alcoxolation alone since water is not produced during this phase. These figures provide no information on the detailed chemistry since an apparent trend associated with base concentration does not exist. We do observe, however, the appropriate experimental trend for the two extreme cases, A and C. Table V gives a clearer summary of the results.

From the FTIR experiments, we can determine the hydrolysis rates, the condensation mechanisms and the resulting products, even though there is a very complex coupling of [OH^-], [H_2O], and [Zr] that is not yet fully understood. Combined with the exceptionally fast hydrolysis, the intrinsic competition between water and base for d^0 orbitals as well as the simultaneous condensation mechanisms that occur, these systems are very difficult to quantify. It is apparent that the rate law depends on [Zr-O-R], [H_2O], and [OH^-] so that is very difficult to predict an overall quantitative rate expression for these reactions. It appears that both water and base are competing for open sites. Partial charge theory combined with experimental results that give more information into the charge and composition of the reaction media at any given time must be employed to give a more thorough analysis of the chemistry and physics of these reactions.

3.3. SAXS results

SAXS experiments were also performed in the present study to help understanding the condensation mechanisms that occurred. The primary parameters that were studied during these experiments were growth kinetics and early-stage structural transitions. That is, Guinier analysis was performed to determine both the size and rate of change of the radius of gyration, and Porod analysis was used to determine the fractal dimensions and the relative structural evolutions during the condensation processes.

Fig. 7 shows the growth kinetics curve of data taken in the Guinier regime at different times along the reaction coordinate for 0.4 M Zr-O-R, 1.1 M H_2O at varying [OH^-]. From observation of the R_g data, it is obvious that particles are growing during the same time that hydrolysis is occurring. That is, during the first seconds of reaction, wherein most of the hydrolysis has occurred according to our previous discussions, we see very rapid particle growth. As hydrolysis data demonstrate a very steep initial slope, condensation growth kinetics also reveal a very steep initial slope in which clusters/particles are being formed from initial oligomers such as zirconium tetramers. Unlike hydrolysis, where it is difficult to elucidate the effect that base has on conversion of Zr-O-R ligands to Zr-OH ligands, the base dependence in the condensation growth curves is more tractable. Fig. 7 shows that a decrease in [OH^-] gives both a faster growth rate, dR_g/dt, and a larger cluster/particle size. Final product sizes for the particles were measured to be ~32–40 Å. This result further demonstrates that hydrolysis and condensation are not isolated events as proposed by Barringer [17]. The values do not increase from these sizes even up to the point of gelation, although gelation clearly illustrates a polymeric network that is visible to the naked eye. For example, the system that gelled in 10 min (A series) had the same R_g value at 9 min as it did at 60 s. This phenomenon was also noted in both B and C series experiments. Gelation was considered to have occurred once a viscous material was visible.

From the analysis of the Porod region, fractal dimensions were determined (see Fig. 8 for the early-stage structural transition data obtained from Porod analyses). Final values for the D_f are 1.8, 1.9, and 2.1 for [OH^-] = 0.01, 0.005, and 0.0025 M, respectively. In this case, it is apparent that the absolute value of the Porod slope increases with decreasing [OH^-]. Since it is commonly known in the literature that base-catalyzed alkoxide gels tend to form more highly branched gels than their acid catalyzed counterparts, this trend is anticipated. That is, the increase in D_f for this series implies that branching is occurring so that the net result goes from a swollen branched polymer, $D_f \sim 2$, to a randomly branched polymer, $D_f \sim 2.2$.

It is possible to utilize the results obtained in the present study to predict an aggregation mechanism. For values of $D_f \sim 2.5$, the growth occurs by a DLA

TABLE V Summary of hydrolysis and condensation of zirconium alkoxides: reaction data after 0.5 s; $[\text{Zr-O-R}]_0 = 0.4$ M and $[H_2O]_0 = 1.1$ M for all samples recorded

(OH^-) (M)	Temp. (°C)	$(H_2O)/(H_2O)_0$	$(\text{Zr-OR})/(\text{Zr-OR})_0$	Apparent condensation mechanism
	10	0.5	0.3	Oxolation and alcoxolation: (H_2O) rises steadily but not drastically
0.01	23	0.76	0.3	Oxolation (drastic rise in (H_2O) after 100 ms)
	34	0.46	0.24	Oxolation and alcoxolation ((H_2O) changes steadily)
	10	0.74	0.36	Oxolation
0.005	23	0.91	0.24	Oxolation: very drastic change in (H_2O)
	34	0.76	0.12	Oxolation
	10	0.86	0.24	Oxolation
0.0025	23	0.72	0.13	Alcoxolation (H_2O) does not change after 100 ms)
	34	0.8	0.09	Alcoxolation

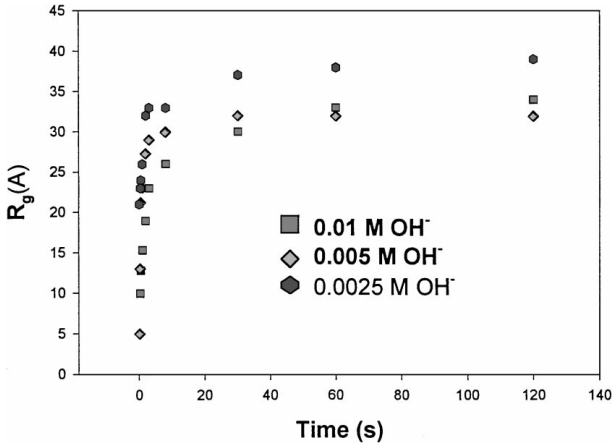

Figure 7 Cluster/particle growth kinetics for 0.4 M Zr-OR, 1.1 M H_2O at varying (OH^-).

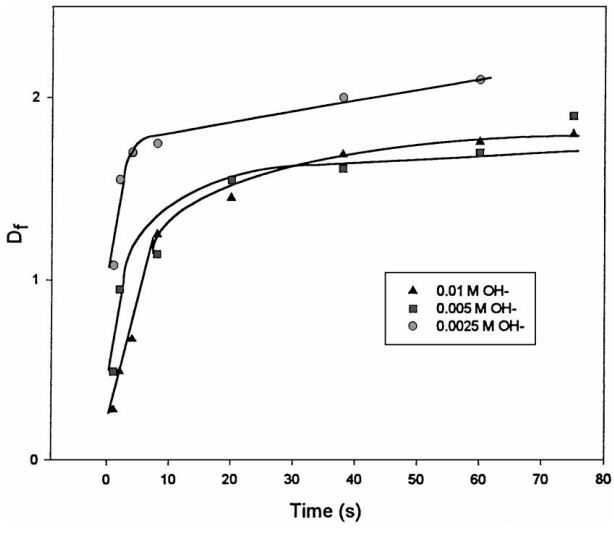

Figure 8 Microstructural transition with time during gelation from solutions containing 0.4 M Zr-OR, 1.1 M H_2O, at 23°C and varying (OH^-).

scheme [9]. Therefore, the data indicate that these primary particles grow by RLA, in which chemistry plays more of a role in aggregation than in a case that is mass-transfer controlled. The fact that the R_g does not increase even up to gelation, although the gel network is visibly becoming larger, adds evidence to the fact that the initial growth occurs by a condensation mechanism that it is governed by RLA phenomena. That is, the gels are constructed with polymeric units or clusters that are of the same size dimensions as the final R_g sizes. Because these eventually form gels that are visible to the naked eye, it is obviously incorrect to conclude that the gel network is of these dimensions. Therefore, it is reasonable to conclude that the initial burst of R_g is due to the hydrolysis and condensation reactions. Subsequent growth then occurs by DLA, wherein these monomeric or oligomeric clusters collide and stick together to form the resultant gels. DLVO and intermolecular forces ultimately determine the outcome of these diffusion processes [41].

This is, again, verified by the experimentally determined values of D_f for the primary particles. Literature values of $D_f < 2.1$ indicate that the growth mechanism for primary particles occurs by reaction rather than by diffusion [9]. Then, too, it can be seen from the Zr-OR percent-conversion plots that (a) the elimination of -OR groups is not a complete reaction during the initial stages of hydrolysis, and (b) (H_2O) appears to grow or fluctuate during this same period of time. These results suggest that chemical reactions are occurring while primary particles are being formed. From the plots, we also see that residual amounts of -OR groups are always present. In time, however, the relative concentration of these residual groups eventually decreases with respect to the hydroxolated moieties. It is assumed that these residual amounts are related to the steric hindrance of the particles as they grow. As the alkoxy groups are more completely hydrolyzed, less steric hindrance will be observed on the individual polymeric species. A less sterically hindered species has less resistance to traverse and, thus, grow by DLA. Therefore, it is apparent from the FTIR and SAXS data that a combination of RLA and DLA processes are involved in the production of these zirconia oxide gels.

4. Summary

A continuous, flow-through, rapid-mixing technique was successfully adapted and developed in this study to investigate the hydrolysis and condensation of

zirconium *n*-tetrabutoxide by FTIR and SAXS. Data collection as early as 100 ms was achieved. For the first time, we have been able to experimentally investigate the earliest-stage processes of zirconium butoxides gelation, catalyzed by quaternary tetramethyl ammonium hydroxide in ethanol. Combining both FTIR data and SAXS data, we determined that hydrolysis and condensation are overlapping reactions. Nevertheless, the majority of the hydrolysis is completed within 1 s. During this same time, condensation is also occurring. The condensation mechanisms were determined to consist of both alcoxolation and oxolation. That is, during the reaction, the water concentration initially decreased due to hydrolysis and then either fluctuated or reached a steady-state value. From these data, it was concluded that the former case involved condensation via an oxolation mechanism and that the latter case suggested an alcoxolation mechanism.

As predicted from classical chemical engineering reaction kinetics, the increase of temperature drove the hydrolysis reactions faster. Since the percentage change in (Zr-O-R) ligand was much greater in the first 100 ms than for the rest of the reaction, hydrolysis was modeled as a first-order reaction in substrate. Although the reaction did proceed at a more rapid rate with an increase in temperature, the hydrolysis did not proceed faster for greater $[H_2O]/[OH^-]$, although the gelation time increased significantly. This information led us to conclude that OH^- plays a major role in competing with water for the empty d^0 orbitals of the Zr-O-R ligands since the lowest and highest ratios exhibited this behavior but the middle ratio did not. In this sense, OH^- does not behave as a "true" catalyst. Further experiments must be performed that detail the charge analysis during the reaction in order to fully grasp the detailed chemistry and to determine how the $[OH^-]$ affects the hydrolysis conversion.

A more definable trend occurred with the kinetic growth data as the reaction proceeded through a condensation mechanism. SAXS analysis revealed that, with decreasing base concentrations, the primary particles both grew faster and were larger in size. Also, it was determined that with less base the fractal dimensions increased. This increase in D_f for the series implies that branching is occurring and that these particles are less dense than their acid-catalyzed counterparts. It was concluded that the polymeric clusters are formed from an RLA mechanism as opposed to a DLA mechanism. However, once these primary particles are formed, condensation does proceed by cluster diffusion.

Acknowlegement

This research is supported by the U.S. Department of Energy, Basic Energy Sciences, Division of Material Sciences. The submitted manuscript has been authored by a contractor of the U.S. Government under contract No. DE-AC05-96OR22464. Accordingly, the U.S. Government retains a nonexclusive, royalty-free license to publish or reproduce the published form of this contribution, or allow others to do so, for U.S. Government purposes.

References

1. L. L.HENCH and J. K. WEST, *Chem. Rev.* **90** (1990) 33.
2. L. C. KLEIN, "Sol-Gel Technology for Thin Films, Fibers, Preforms, Electronics and Specialty Shapes" (Noyes Pub., New York, 1988).
3. J. LIVAGE, M. HENRY and C. SANCHEZ, *Prog. Solid St. Chem.* **18** (1988) 259.
4. B. E. YOLDAS, *J. Mater. Sci.* **21** (1986) 1080; *J. Non-Cryst. Solids* **81** (1986) 365.
5. K. D. BUDD, S. K. DEY and D. A. PAYNE, *Mater. Res. Soc. Symp.* **73** (1986) 711.
6. R. W. HARTEL and K. A. BERGLUND, in "Better Ceramics Through Chemistry II," edited by C. J. Brinker, D. E. Clark and D. R. Ulrich (Mater. Res. Soc., Pittsburgh, Pa., 1986). *Mater. Res. Soc. Symp. Proc.* **73** (1986) 633.
7. J. BLANCHARD, S. BARBOUX-DOEUFF, J. MAQUET and C. SANCHEZ, *New J. Chem.* **19** (1995) 929.
8. J. SANCHEZ and A. MCCORMICK, *J. Phys. Chem.* **96** (1992) 8973.
9. C. J. BRINKER and G. W. SCHERER, "Sol-Gel Science: The Physics and Chemistry of Sol-Gel Processing" (Academic Press, Inc., Boston, 1990).
10. J. L. LOOK and C. F. ZUKOSKI, *J. Colloid Inter. Sci.* **153** (1992) 461.
11. M. T. HARRIS, O. A. BASARAN and C. H. BYERS, *Mat. Res. Soc. Symp. Proc.* **271** (1992) 291.
12. M. T. HARRIS and C. H. BYERS, *J. Non-Cryst. Solids* **103** (1988) 49.
13. K. KUSTIN, "Methods in Enzymology, XVI: Fast Reactions" (Academic Press, London, 1969).
14. M. T. HARRIS, A. SINGHAL, J. L. LOOK, J. R. SMITH-KRISTENSEN, J.-S. LIN and L. M. TOTH, *J. Sol-Gel Sci. Technol.* **8** (1997) 41.
15. D. BRADLEY and D. CARTER, *Can. J. Chem.* **39** (1961) 1434.
16. D. D. BRADLEY, R. C. MEHROTRA and D. P. GAUR, "Metal Alkoxides" (Academic, London, 1978).
17. E. A. BARRINGER and H. K. BOWEN, *Langmuir*, **1** (1985) 414.
18. H. KUMAZAWA, T. INOUE and E. SADA, *Chem. Eng. J.* **55** (1994) 93.
19. A. SINGHAL, L. M. TOTH, J. S. LIN and K. AFFHOLTER, *J. Am. Chem. Soc* **118** (1996) 11529.
20. J. GUILMENT, O. PONCELET, J. RIGOLA and S. TRUCHET, *Vibrational Spectroscopy* **11** (1996) 37.
21. P. M. SMIT, A. V. ZYL and A. I. KINGON, *Mater. Chem. Phys.* **17** (1987) 507.
22. A. SINGHAL, L. M. TOTH, M. T. HARRIS and M. Z.-C. HU, *Journal of Non-Crystalline Solids* **246** (1999) 197.
23. R. H. PERRY and C. H. CHILTON, "Chemical Engineers' Handbook, 5th ed." (McGraw-Hill Book Company, New York, 1972).
24. R. W. HENDRICKS, *J. Appl. Phys.* **11** (1978) 15.
25. D. W. SHAEFER and K. D. KEEFER, in "Better Ceramics Through Chemistry," edited by C. J. Brinker, D. E. Clark and D. R. Ulrich (Elsevier/ North Holland, New York, 1984). *Mater. Res. Soc. Symp. Proc.* **32** (1984) 1.
26. K. D. KEEFER, in "Better Ceramics Through Chemistry II," edited by C.J. Brinker, D.E. Clark and D.R. Ulrich (Elsevier/North Holland, New York, 1984). *Mater. Res. Soc. Symp. Proc.* **73** (1986) 295.
27. A. GUINIER and G. GOURNET, "Small Angle Scattering of X-Rays" (John Wiley and Sons, New York, 1955).
28. P. W. SCHMIDT, F. EHRBURGER-DOLLE and D. J. VOSS, *Mat. Res. Soc. Symp. Proc.* **407** (1996).
29. J. E. MARTIN and A. J. HURD, *J. Appl. Cryst.* **20** (1987) 61.
30. A. MILLER, "Writing Reaction Mechanisms in Organic Chemistry" (Academic Press, London, 1992).
31. V. DAY, T. EBERSPACHER, A. TODD and W. KLEMPERER, *Chem. Process. Adv. Mater.* **257** (1992).
32. R. T. SANDERSON, *Science* **114** (1951) 670.
33. R. J. HUNTER, "Foundations of Colloid Science" (Clarendon Press, Oxford Press, 1987).
34. R. N. ISRAELACHIVILLI, "Intermolecular and Surface Forces" (Academic Press, London, 1985).

35. D. F. EVANS, "The Colloidal Domain" (VCH Publishers, Inc., Toronto, 1994).
36. M. V. SMOLUCHOWSKI, *Z. Phys. Chem.* **92** (1916) 557.
37. T. A. WITTEN and L. M. SANDER, *Phys. Rev. Lett.* **47** (1981) 1400.
38. P. MEAKIN, *ibid.* **51** (1983) 1119.
39. J. KHATOURI, M. MOSTAFAVI and J. BELLONI, *Z. Phys. D*, **34** (1995) 47.
40. H. S. FOGLER, "Elements of Chemical Reaction Engineering" (Prentice Hall, New Jersey, 1992).
41. J. L. LOOK and C.F. ZUKOSKI, *J. Am. Ceram. Soc.* **78** (1995) 21.

Received 11 December 1998
and accepted 5 October 1999